SORPTION OF CESIUM USING KZnFc ON PHOSPHORIC ACID-BASED GEOPOLYMER

#LI-CHING CHUANG, CHI-HUNG LIAO

Division of Chemical Engineering, Institute of Nuclear Energy Research, No.1000, Wenhua Rd., Longtan Township, Taoyuan 325, Taiwan, R.O.C.

#E-mail: jay32000@iner.gov.tw

Submitted February 19, 2015; accepted June 14, 2015

Keywords: Metal ferrocyanide, Granular, Compressive strength, Phosphate geopolymer

The adsorbent was synthesized from the acid-base reaction between metal ferrocyanide and acidic phosphate at room temperature. The metal ferrocyanide granular inorganic adsorbent based on phosphate geopolymer for the removal of cesium in either batch or packed-bed operation has been developed in this study. In this work, the compressive strength of granular inorganic adsorbent was investigated under different liquid-to-solid, metal ferrocyanide-to-geopolymer and MgO-to-KH_2PO_4 ratios. The result showed that the compressive strength of the adsorbent increased with the increase of MgO-to-KH_2PO_4 ratio. It was found that the optimization of metal ferrocyanide-to-geopolymer and MgO-to-KH_2PO_4 ratios was important in improving both the compressive strength and the adsorption capacity of the adsorbent. The metal ferrocyanide granular inorganic adsorbent prepared were characterized by analysis such as XRD, TGA, FTIR and SEM spectra. In this study, the synthesized granular inorganic adsorbent has demonstrated a Cs removal efficiency of over 99 % and an adsorption capacity of 1.7-1.8 meq·g^{-1} in simulation wastewater containing 2000 ppm Cs under adsorbent dose of 0.0067 g·ml^{-1}.

INTRODUCTION

The release of cesium radionuclide into the environment is of concern due to its high solubility characteristics when up-taken by human body though food chain. Moreover, the long half-life of ^{137}Cs (30 years) has made it a highly radiotoxic nuclide. Therefore, removal of cesium radionuclide in wastewater from Nuclear Power Plant (NPP) or nuclear facilities is an important issue for nuclear waste management. Nuclear waste effluents from NPP typically is acidic (i.e. HNO_3) and has high concentration of sodium (i.e. $NaNO_3$) [1]. Special attention has been given to the selective removal of ^{137}Cs from radioactive wastewater containing highly acidic and concentrated sodium. Furthermore, granules suitable for column operation have been prepared by binding or precipitating fine inorganic adsorbent onto porous particles. Among various types of granular inorganic adsorbent, the ferrocyanides of transition metals (II) (Ni, Cu, Zn, Fe and others) demonstrate the highest selectivity towards the removal of cesium from radioactive wastewater [2, 3]. Konecny et al. used porous silica gel particles as substrate to load $K_4Fe(CN)_6$ and then reacted with $ZnSO_4$ to form granular inorganic adsorbent[4]. Shabana et al. used granular porous polymethylmethacrylate as support and loaded with potassium iron(III) hexacyanoferrate(II) [5]. Hitoshi et al. loaded potassium nickel hexacyanoferrates on granular porous chabazite [6]. Hitoshi et al. reported the incorporation of potassium iron (III) hexacyanoferrate (II) crystal on the granular porous support of zeolite [7]. Although above mention granular porous support has good retention capacity for radioactive cesium, they have low mechanical stability and high flow resistance, leading to clogging of the column. In addition, the preparation procedures were complicated and the product was often not reproducible. In order to improve their low mechanical stability and high flow resistance, the fine metal ferrocyanides have been produced by incorporation with some organic binder. Rao et al. used polyvinyl acetate as binder in the preparation of copper (II) ferrocyanide on polyurethane foam support [8]. Someda et al. prepared transition metal ferrocyanides on polyacrylonitrile as binder and support [9]. Even though granular adsorbent within organic binder has good mechanical stability, it might be degraded by radiation and other biological action overtime, resulting in the leakage of radioactive cesium nuclides. In order to overcome the low mechanical stability and high flow resistance of granular adsorbent and avoid using organic

binder, we attempted to combine fine transition metal ferrocyanides powder with geopolymer. Geopolymer is often used for the stabilization/solidification (S/S) of mixed wastes as well as low-level nuclear waste due to its excellent mechanical strength [10-12]. Various types of geopolymer, silicate alkali-based geopolymer [13] and phosphoric acid-based geopolymer [14], have been developed during the last decade. It was reported that the high pH of silicate alkali-based geopolymers may induce the hydrolysis of transition metal ferrocyanides, leading to the destruction of its molecular structure [15]. On the other hand, in phosphoric acid-based geopolymer, the main reaction product is magnesium potassium phosphate hexahydrate or k-struvite ($MgKPO_4 \cdot 6H_2O$)[16], which is formed by the acid-based reaction between burned magnesia and potassium dihydrogen phosphate [11]. In this case, hydrolysis of transition metal ferrocyanides can be avoided. The present study deals with the preparation of zinc ferrocyanide-loaded k-struvite, characterization of this granular inorganic adsorbent, and its uptake property towards ^{137}Cs in simulated wastewater.

EXPERIMENTAL

Material

Potassium ferrocyanide trihydrate ($K_4[Fe(CN)_6] \cdot 3H_2O$) and zinc sulfate heptahydrate ($ZnSO_4 \cdot 7H2O$) were used as received for the preparation of zinc ferrocyanide powder [17]. Sintered magnesium oxide (MgO), potassium hydrogen phosphate (KH_2PO_4) and boric acid were used as received for the preparation of phosphoric acid-based geopolymer which then mixed with KZnFC [18]. DT-30A (commercial granular inorganic adsorbent, Diversified Technologies Services, Inc.) was used for comparison in terms of distribution coefficient, adsorption capacity and compressive strength.

Preparation of Potassium zinc ferrocyanide powder (KZnFC) [17]

The KZ41, KZ21, KZ11, KZ12 and KZ14 were designated for the prepared KZnFC with $K_4[Fe(CN)_6] \cdot 3H_2O$ (1M)-to-$ZnSO_4 \cdot 7H_2O$ (1M) volume ratio of 4:1, 2:1, 1:1, 1:2 and 1:4, respectively. For instance, the preparation of KZ41 is as follows. 73.67 g of $K_4[Fe(CN)_6] \cdot 3H_2O$ (1 M), and 14.378 g of $ZnSO_4 \cdot 7H_2O$ (1M) were added into 200 ml, and 50 ml of deionized water, respectively. Then, $K_4[Fe(CN)_6] \cdot 3H_2O$ solution was added into $ZnSO_4 \cdot 7H_2O$ solution dropwisely followed by stirring for 7 days at room temperature to form white slurry. Finally, the resulting slurry was washed by deionized water followed by centrifuge and dried in vacuum at 80°C for 2 h to obtain KZ41. Similar method was used to obtain KZ21, KZ11, KZ12 and KZ14.

Preparation of phosphoric acid-based geopolymer for granulation of KZnFC

Adjustment of MgO-to-KH_2PO_4 mass ratio

The MK11, MK21, MK31, MK41 and MK51 were designated for the prepared KZnFC granules via phosphoric acid-based geopolymer with MgO-to-KH_2PO_4 mass ratio of 1:1, 2:1, 3:1, 4:1 and 5:1, respectively. For instance, the preparation procedure for MK51 is as follows. 8.23 g of MgO, 1.65 g of KH2PO4, 10 g of KZnFC and 0.12 g of Boric acid were first mixed by milling for 2 hr. Then, 12 ml of de-ionized water was added slowly into the premixed power while stirring. Stirring of the slurry was kept for 5 min and then it was poured into a mold for hardening. After hardening, compressive strength of the bulk was measured. To test the removal efficiency for Cs, the solidified KZnFC bulk was crushed and sieved to obtain granular KZnFC adsorbent with particle size of 1-2 mm. Prior to adsorption test, the granular KZnFC adsorbents were washed to remove fine powder by deionized water and dried at 60°C for 24 hr. Similar method was used to obtain MK21, MK31, MK41 and MK51.

Adjustment of KZnFC-to-geopolymer mass ratio

The KC11, KC21, KC41 and KC61were designated for the prepared KZnFC granules with KZnFC-to-geopolymer mass ratio of 1:1, 1.2:1, 1.4:1 and 1.6:1, respectively. For instance, the preparation procedure for K11 is as follows. 9.88 g of geopolymer (containing MgO and KH_2PO_4 with mass ratio of 2:1 or 3:1), 10 g of KZnFC and 0.12 g of Boric acid were first mixed by milling for 2 hr. Then, 12 ml of de-ionized water was added into the premixed power while stirring. Stirring of the slurry was kept for 5 min and then it was poured into a mold for hardening. After hardening, compressive strength of the bulk was measured. To test the removal efficiency for Cs, the solidified KZnFC bulk was crushed and sieved to obtain granular KZnFC adsorbent with particle size of 1 - 2 mm. Prior to adsorption test, the granular KZnFC adsorbents were washed to removed fine powder by deionized water and dried at 60°C for 24 hour. Similar method was used to obtain KC21, KC41 and KC61.

Characterization

X-ray diffraction (XRD) spectra were obtained on a D8 ADVANCE using Cu Kα radiation (45 kV and 40 mA). Infrared spectra were collected using TENSOR 70 Fourier transform infrared spectroscopy (FTIR). X-ray diffraction (XRD) spectra were obtained on a D8 ADVANCE using Cu Kα radiation (45 kV and 40 mA).

Thermogravimetric analysis (TGA) was obtained on a STA 409PC (NETZSCH). The compressive strength of the samples was measured using a mechanical tester (HT-2402) with granular adsorbent particle size of around ψ 6 × 11 mm. At least 10 sample were tested in the mechanical test with loading speed is 20 mm·min^{-1}. Scanning electron microscopy (SEM, JEOL JSM-6701F) was used to characterize the morphology of the specimens.

Batch adsorption test for the prepared adsorbents

The adsorption capacity of adsorbent was calculated as

$$Q\ (\text{meq g}^{-1}, \text{mole g}^{-1}) = \frac{(C_0 - C) \times V}{W \times M} \quad (1)$$

where C_0 is initial cesium concentration (ppm), C is the final cesium concentration (ppm) in the solution, V is the volume of simulated solution (l), M is the cesium molecular weight (g·mol^{-1}), W is the weight of adsorbent (g).

The cesium removal efficiency (R, %) of adsorbent in the simulated solution was determined as [19]

$$R\ (\%) = \frac{(C_0 - C) \times 100}{C_0} \quad (2)$$

where C_0 is initial cesium concentration (ppm), C is the final cesium concentration (ppm) in the solution.

To perform the adsorption test, 0.2 g of powder KZnFC or granular adsorbent was added to the simulated cesium ion solution (2000 ppm, 30 ml, $CsNO_3$, 0.0067 g·ml^{-1}). The mixture solution was shaken on a rotary shaker at 25°C for 24 h. When the adsorption test was completed, the mixture solution was centrifuged at 4000 rpm for 30 min. The supernatant liquid was measured by atomic absorption spectrometer (iCE 3300) to determine the residual cesium ion concentration. In addition, short-term adsorption tests were performed for the prepared adsorbents. Here, 0.2 g of powder KZnFC or granular adsorbent was added to the simulated cesium ion solution (2000 ppm, 30 ml, $CsNO_3$). The mixture solution was shaken on a rotary shaker at 25°C for 2, 5, 10, 30, 60, and 120 min.

RESULTS AND DISCUSSION

Potassium zinc ferrocyanide powder (KZnFC)

Figure 1 shows the time-dependent cesium uptake (mole·g^{-1}) for various powder KZnFCs. The result shows that the amount of adsorbed cesium ion approached equilibrium within 2 h for all adsorbents. Among them, ZK11 shows the highest cesium uptake, suggesting that too high or too low $K_4[Fe(CN)_6]\cdot 3H_2O$-to-$ZnSO_4\cdot 7H_2O$ ratio may not benefit the cesium uptake of the adsorbents. It was reported that the high $K_4[Fe(CN)_6]\cdot 3H_2O$-to-$ZnSO_4\cdot 7H_2O$ ratio is favorable to give a high yield of $K_2Zn_3[Fe(CN)_6]_2$ [2] and the cesium uptake of $K_2Zn_3[Fe(CN)_6]_2$ is higher than that of $Zn_2Fe(CN)_6$ [20], attributing to the improved the ion exchange rate of the cesium ion with the potassium ion [17]. In contrary, excess $K_4[Fe(CN)_6]\cdot 3H_2O$-to-$ZnSO_4\cdot 7H_2O$ mole ratio will leave excess potassium ions in solution which may restrict the ion exchange of cesium ion by $K_2Zn_3[Fe(CN)_6]_2$ [21]. The above-mentioned result shows that ZK11 has higher uptake of cesium among the adsorbents tested, especially in a short period of adsorption time, meaning it requires less residence time when applies in the column. In addition, ZK11 exhibits an adsorption capacity of 1.88 meq·g^{-1}, which is higher than that of the commercial adsorbent, DT-30A, (1.5 meq·g^{-1}) for an adsorption time of 2 hr. Therefore, ZK11 was selected for the granulation of KZnFC via phosphoric acid-based geopolymer.

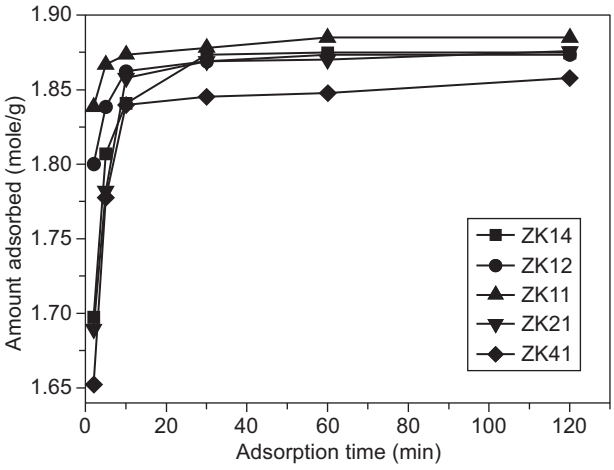

Figure 1. Time-dependent cesium uptake (mole·g^{-1}) for powder KZnFC.

Effect of MgO-to-KH_2PO_4 mass ratio for the preparation of granular KZnFC adsorbents

Compressive strength

The mechanism of phosphoric acid-based geopolymer formation involves Mg^{2+}, K^+ and PO_3^{-4} existed in the solution at the specific value of pH according to the Equation 3 [11, 22]:

$$Mg^{2+} + K^+ + PO_3^{-4} + 6H_2O \rightarrow MgKPO_4\cdot 6H_2O \quad (3)$$

First, KH_2PO_4 was dissolved by the added water to release H^+, which initializes the hydration reaction. Then, MgO begins to dissolve, increasing the pH value of the mixture. When the pH value is over 7, $MgKPO_4\cdot 6H_2O$

is formed. Figure 2 shows the compressive strength of the geopolymer with different MgO-to-KH_2PO_4 mass ratios. It is found that the compressive strength of geopolymer increases with the increase of MgO-to-KH_2PO_4 mass ratios. The largest compressive strength value was about 35.32 MPa for MK51 with the MgO-to-KH_2PO_4 mass ratios of 5:1. This may be due to that fact that the geopolymer of MK51 not only composed of the hydrated product, but also excess residual MgO particle. Such residual MgO particles may improve the compressive strength of the geopolymer. It was reported that the higher MgO content may brought much more internal stress in sample lead to fast setting [23].

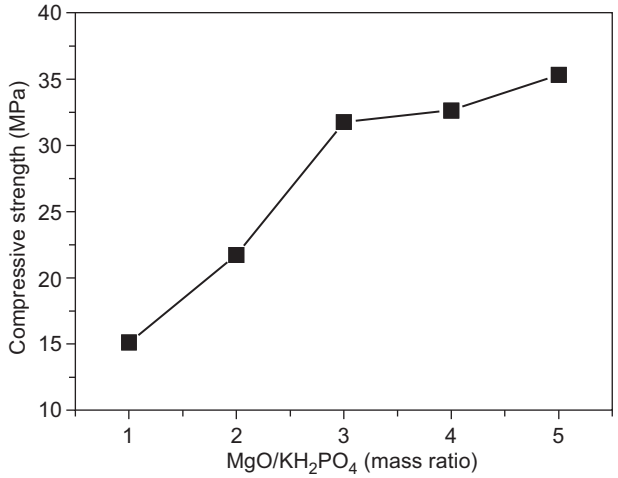

Figure 2. Compressive strength of the geopolymer with different MgO-to-KH_2PO_4 mass ratios.

XRD diffraction patterns

The increase of compressive strength with increase of MgO-to-KH_2PO_4 mass ratios can also be explained by the XRD patterns of the samples as shown in Figure 3. The diffraction peaks of KH_2PO_4, MgO, KZnFC (KZ11) and $MgKPO_4{\cdot}6H_2O$ (MKP) are noted for MK11 with the MgO-to-KH_2PO_4 mass ratios of 1:1. The intensity of the diffraction peak representing KH_2PO_4 decreases with the increase of the MgO-to-KH_2PO_4 mass ratios, suggesting that the crystallinity of $MgKPO_4{\cdot}6H_2O$ was affected by the content of MgO. This is mainly attributed to the pH-dependent nature of the nucleation and growth of hydrated product [23]. For the case of the MK51, the excess amount of MgO added results in a rapid increase of pH value, leading increase in the nucleation rate. Since there was not enough time for the precipitated $MgKPO_4{\cdot}6H_2O$ to crystallize, amorphous phase was observed for MK51. On the other hand, in the case of MK11, the pH value increased slowly, providing enough time for the precipitated $MgKPO_4{\cdot}6H_2O$ to crystallize [23]. Therefore, with the increase of the MgO-to-KH_2PO_4 mass ratios, the amount of crystallized phase decreased while the amount of amorphous phase increased.

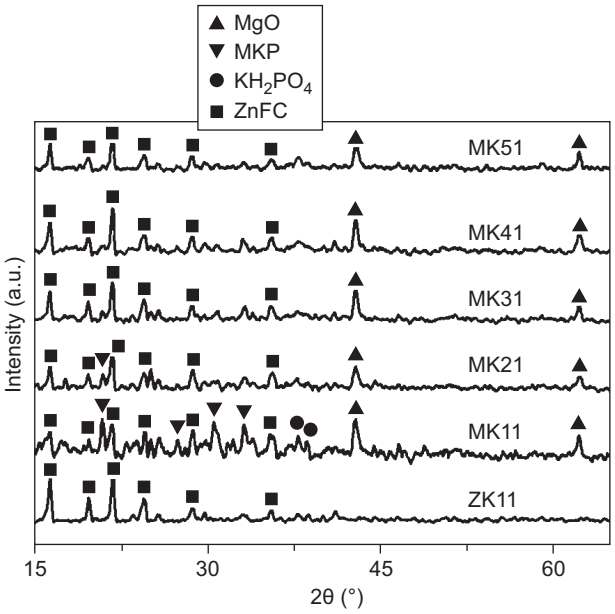

Figure 3. XRD diffraction patterns of granular KZnFC adsorbents with different MgO-to-KH_2PO_4 mass ratios.

Thermogravimetric analysis (TGA)

Thermogravimetric analysis (TGA) of MgO, KZnFC, $MgKPO_4{\cdot}6H_2O$ were obtained as shown in Figure 4. The MgO shows a total weight loss of 8 % from 353°C to 461°C, indicating decomposition of magnesium hydroxide to magnesium oxide due to a few of MgO was hydrolyzed to magnesium hydroxide during storage [24]. As shown in Figure 4b, the thermograms indicate four different weight loss ranges: 100 - 150°C, 150 - 268°C, 575 - 914°C and above 914°C. This first weight loss is associated with the loss of water adsorbed on the surface of the KZnFC and water of crystallization.

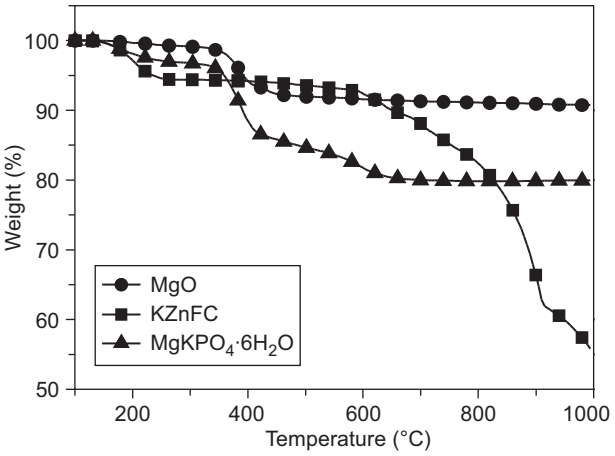

Figure 4. Thermogravimetric analysis of: a) MgO, b) KZnFC, c) $MgKPO_4{\cdot}6H_2O$.

The second weight loss is attributed to the decomposition of KZnFC to the intermediate products, K_2CO_3, ZnO and $ZnFe_2O_4$ [19]. In the third weight loss, evolution of gaseous compounds such as CO_2, NO, and NH_3 [25] may take place. For the final weight loss at temperature above 850°C, decomposition of K_2CO_3 to K_2O [19] may occur. The thermogram of KZnFc is similar to that of KCoFc and KNiFc. As shown in Figure 4c, $MgKPO_4{\cdot}6H_2O$ shows weight loss from temperature of 142°C to 278°C, attributing to the release crystallized water. In addition, the $MgKPO_4{\cdot}6H_2O$ shows a total weight loss of 12 % from 343°C to 629°C, indicating decomposition of magnesium hydroxide to magnesium oxide due to residual MgO in $MgKPO_4{\cdot}H_2O$. Figure 5 shows the TGA profile for the granular inorganic adsorbents with different MgO : KH_2PO_4 mass ratios, the weight loss profile of all samples are almost identical for $MgKPO_4{\cdot}H_2O$, MgO and KZnFc. In addition, the weight loss of MgO increased with the increase of the MgO content in adsorbents. The result indicated that the transition metal ferrocyanides(ZnFC) is stable druing the geopolymerization process.

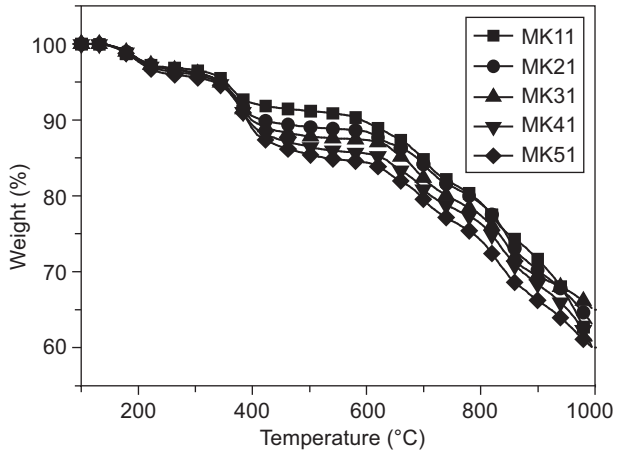

Figure 5. Thermogravimetric analysis of granular inorganic adsorbents with different MgO : KH_2PO_4 mass ratios.

Fourier transform infrared spectroscopy (FTIR)

Figure 6a shows the FTIR spectra for MgO, $MgKPO_4{\cdot}H_2O$ and KZnFC. There are two types of OH bonding exist in MgO. First, is the O–H stretching and bending bonded with Mg and second is the O–H stretching and bending attached at the surface of the samples. The O–H stretching bonded with Mg will be appeared as a transmittance peaks at 3699 cm^{-1} and 1494 cm^{-1}. For the second O-H stretching, it appears as a broad band at 3600 - 3200 cm^{-1}. This occurrence happens due to the special characteristic of MgO, which may adsorb moisture from the ambient [26]. As shown in Figure 6c, the KZnFc shows transmittance peaks at 2094 cm^{-1} corresponding to the C–N groups in hexacyanoferrate (II). The broad transmittance peaks revealed in 3600 - 3200 cm^{-1} region were assigned to –OH stretching of hydrogen bonded water molecules. In addition, the presence of coordinated water molecules existing in the interlayer structure of KZnFc was detected around 1600 cm^{-1} [27]. As shown in Figure 6b, the $MgKPO_4{\cdot}H_2O$ (MK51) shows transmittance peaks at 1053 cm^{-1} and 3600 - 3200 cm^{-1}, corresponding to PO_4^{3-} and –OH groups [28]. Furthermore, the O-H stretching bonded with the special characteristic of residual MgO in $MgKPO_4{\cdot}H_2O$ shows transmittance peaks at 3699 cm^{-1} and 3600 - 3200 cm^{-1}. Figure 7 shows the FTIR spectra for granular inorganic adsorbents with different MgO:KH_2PO_4 mass ratios, the transmittance peaks of all samples are almost identical for $MgKPO_4{\cdot}H_2O$ and KZnFc. The result indicated that the main reaction product of phosphoric acid-based geopolymer is magnesium

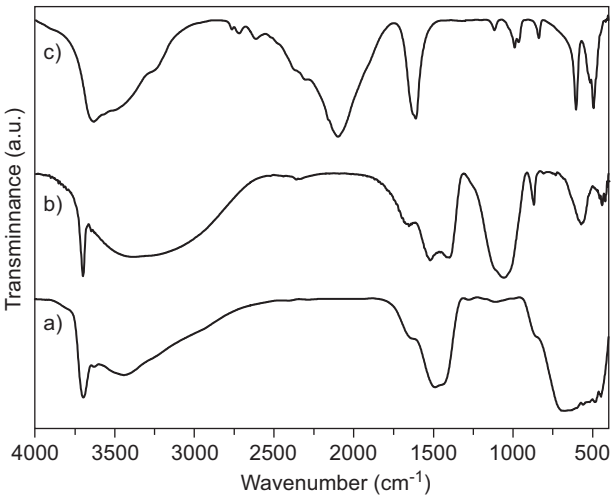

Figure 6. FTIR spectra of a) MgO, b) $MgKPO_4{\cdot}H_2O$, c) KZnFC.

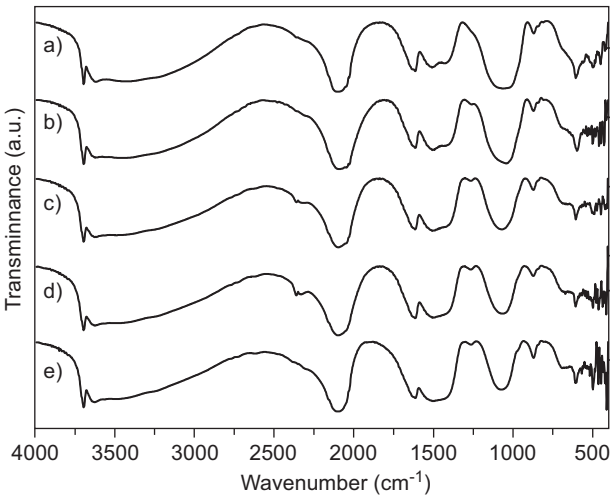

Figure 7. FTIR spectra of granular inorganic adsorbents with different MgO : KH_2PO_4 mass ratios.

potassium phosphate hexahydrate or k-struvite ($MgKPO_4 \cdot 6H_2O$)[16], which is formed by acid-based reaction between burned magnesia and porassium dihydrogen phosphate [11]. The hydrolysis of the transition metal ferrocyanides during the geopolymerization process can be avoided. Therefore, the phosphoric acid-based geopolymer has shown great chemical stability when KZnFc is used in the preparation.

Scanning electron microscopy (SEM)

Figure 8 shows SEM micrographs of the microstructures of granular inorganic adsorbents with different MgO : KH_2PO_4 mass ratios. As shown in Figure 8a, it can be seen that a large amount of pores could be found in the granular inorganic adsorbents. With the MgO:KH_2PO_4 mass ratio increased to 3:1, the pores were gradually formed with lots of agglomerations compo-sed of fragmental lamellar crystalline cluster as shown in Figure 8b. Finally, when the mass ratio of MgO:KH_2PO_4 reached 5:1, the fragmental lamellar crystalli-ne clusters formed crystalline structure sheets as depicted in Figure 8c. According to Griffith Crack Theory [29], the stress concentration factor for the microstructures with a larger amount of pores is higher than that with small ones. This indicated that excess MgO would result in less pores due to that residual MgO as the core material could slow down the nucleation of $MgKPO_4 \cdot 6H_2O$, leading to low stress concentration. Meanwhile, the lowered stress concentration factor would result in the high compressive strength corresponding to more compact sheet crystalline structure. Therefore, increasing the MgO : KH_2PO_4 mass ratio of granular inorganic adsorbents would result in low pore density and low stress concentration factor, leading to the formation of compact sheet crystalline structure with higher compressive strength.

Adsorption capacity

The effect of MgO-to-KH_2PO_4 mass ratios on Cs ion adsorption is shown in Figure 9. The maximum adsorption capacity for MK11, MK21, MK31, MK41 and MK51 is 1.77, 1.6, 1.47, 1.35, and 1.32 $meq \cdot g^{-1}$, respectively. The adsorption capacity was increased with the decrease of MgO-to-KH_2PO_4 mass ratios. In contrast, the compressive strength was increased with the increase of MgO-to-KH_2PO_4 mass ratios as result of more compact granular inorganic adsorbents formed. Yue et al. [30] reported that high adsorption capacity have been achieved resulting from the rigidly open pore structure and extremely high surface area of the immobilization of copper ferrocyanide on granular porous ceramic support, which suggests that the more compact the granular inorganic adsorbent was, the less porous the granular inorganic adsorbent was. Therefore, the internal surface area of $K_2Zn_3[Fe(CN)_6]_2$ (ZK11) may not be as high as that of MK51, resulting in low adsorption capacity. To optimize both the mechanical stability and the adsorption capacity, MK21 and MK31 were selected to run the subsequent tests.

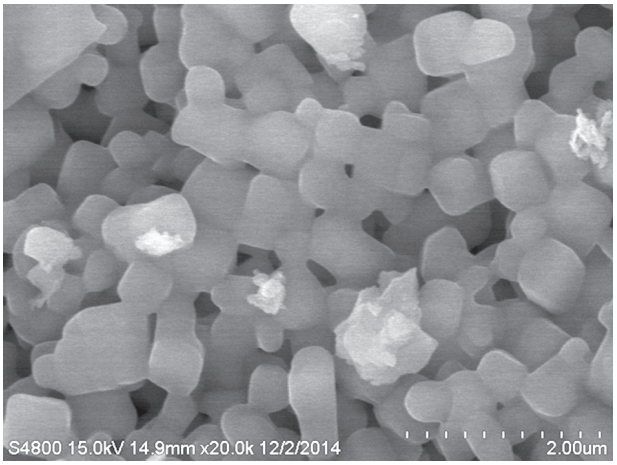

a)

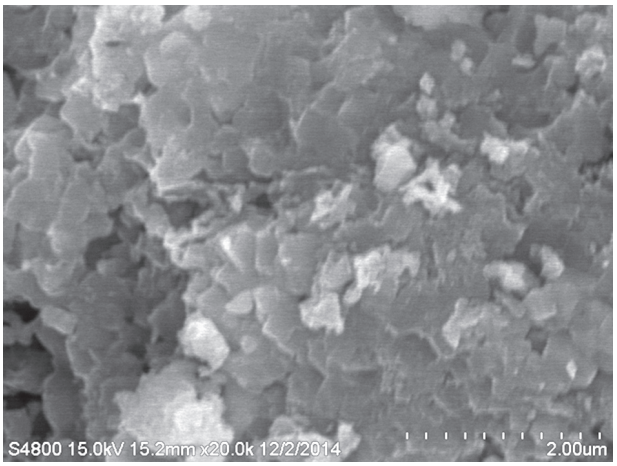

b)

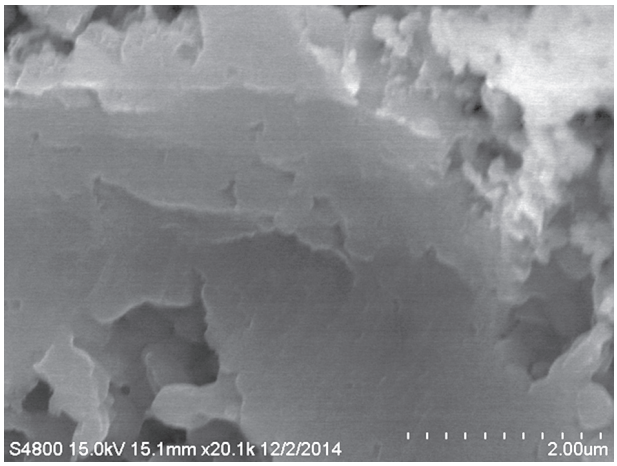

c)

Figure 8. SEM micrographs of granular inorganic adsorbents with different MgO : KH_2PO_4 mass ratios a) 1:1; b) 3:1; c) 5:1.

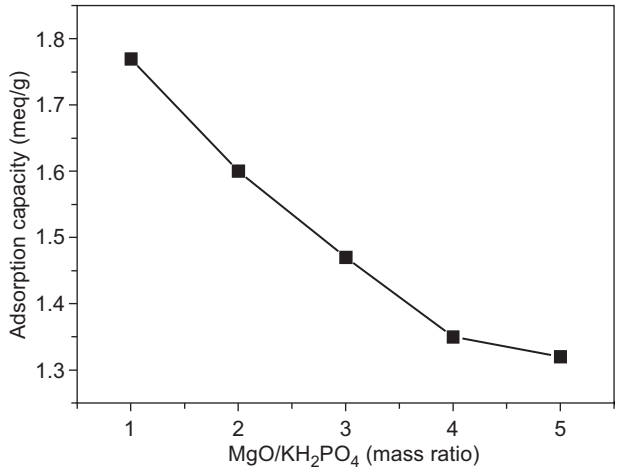

Figure 9. Adsorption capacity of granular KZnFc adsorbents with different MgO-to-KH_2PO_4 mass ratios.

Effect of KZnFc-to-geopolymer mass ratio for the prepared granular KZnFC adsorbents

Adsorption capacity and compressive strength

In order to improve the adsorption efficiency of MK21 and MK31, KZnFc content was increased for the preparation of granular inorganic adsorbents. Figure 10 shows results of the adsorption experiment. The amount of adsorbed cesium ions for MK21 increases with the increase of KZnFc-to-geopolymer mass ratios, reaching a maximum at the mass ratio of 1.4. On the other hand, the maximum adsorption for MK31 is at the KZnFC-to-geopolymer ratio of 1.2. The drop of adsorption capacity may be due to the excess KZnFC blocking the pore sites of the granular adsorbents, leading to decrease in contacting surface area with the solution. Since MK21 may have more pore sites than MK31, more KZnFc can be loaded on MK21 than on MK31, leading to higher adsorption capacity of MK21-KC41 (1.8 meq·g^{-1}) than MK31-KC21 (1.6 meq·g^{-1}). Figure 11 shows the compressive strength of granular KZnFC adsorbents with different KZnFcto-geopolymer mass ratios. It can be seen that the compressive strength of MK31 and MK21 decreased with the increase of KZnFc-to-geopolymer mass ratios. Since geopolymer is a hardening agent, reduce its content may decrease the compressive strength.

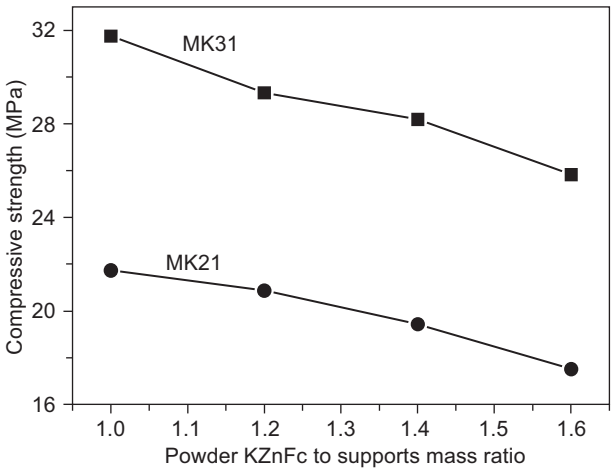

Figure 11. Compressive strength of the bulk with different KZnFc-to-geopolymer mass ratios.

Effect of contacting time on Cs absorption under various Cs concentrations

The adsorption of cesium ion on MK21-KC41 granular inorganic adsorbents was examined at different concentrations of Cs (10 ppm, 100 ppm, 1000 ppm, 2000 ppm) as a function of contacting time at room temperature as shown in Figure 12. With the increase of the contacting time, the cesium ion uptake increased

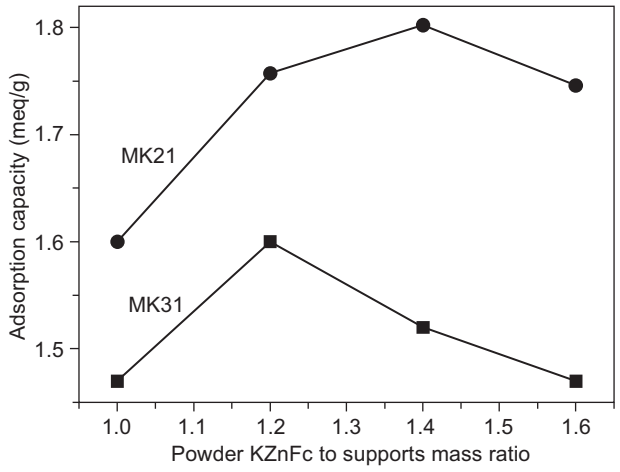

Figure 10. Adsorption capacity of granular KZnFC adsorbents with different KZnFc-to-geopolymer mass ratios.

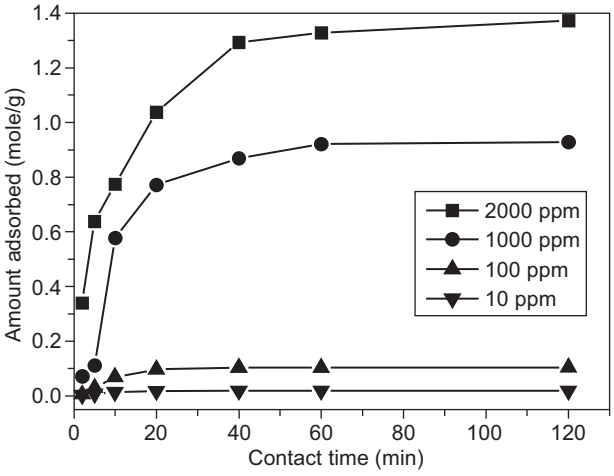

Figure 12. Time-dependent adsorption of cesium on MK21-KC41 under various Cs concentrations.

and remained constant after the equilibration time of 60 min. The amount adsorbed at equilibrium increases from $1.86 \cdot 10^{-2}$ to 1.37 (mole·g^{-1}) with the increase in concentration over the range 10 to 2000 ppm. However, the percentage of cesium ion adsorption increased from 49.5 to 99.28 % with the decrease of initial concentration in the range from 2000 to 10 ppm. The result suggests that the availability of larger sorbent surface sites for a relatively smaller number cesium ions at low initial concentration. The smooth and continuous curves reveal that uptake is initially fast, becoming slower later on and ultimately reaches saturation. Furthermore, the cesium ions preferentially occupy many of active sites of MK21-KC41 in a random manner results in the rapid adsorption rate initially. As time went by, the rate of uptake became slower and eventually reached a constant value due to the saturation of the adsorption surface.

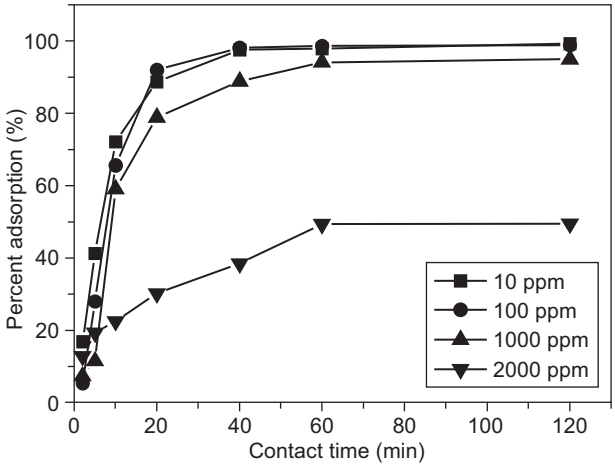

Figure 13. Time-dependent cesium adsorption efficiency on MK21-KC41 under various Cs concentrations.

Adsorption isotherms

The distribution of metal ions between the liquid phase and solid phase can be described by mathematical model equation such as the Langmuir and Freundlich isotherm models. This relates adsorption capacity (*qe*) to the equilibrium adsorbate concentration (C_e) in the bulk fluid phase.

Langmuir adsorption isotherm

The Langmuir adsorption isothermal is the simplest theoretical model for monolayer adsorption with constant heat of adsorption for all sites and without interaction between adsorbed molecules. It suggests a finite number of identical surface sites on the surface of adsorbents. In addition, the model assumes uniform energies of adsorption onto the surface and no transmigration of the adsorbate. The Langmuir isotherm is represented by the following equation: [31]

$$\frac{C_e}{q_e} = \frac{1}{Q_0 b} + \frac{C_e}{Q_0} \quad (4)$$

where *Ce* is the equilibrium concentration (mole·l^{-1}), *qe* is the amount of the cesium ion adsorbed at equilibrium (mole·g^{-1}) and Q_0 and *b* are Langmuir constants relate to the adsorption capacity and the energy of adsorption, respectively.

The plots of *Ce/qe* vs. *Ce* are found to be linear which indicate that the adsorption of cesium ion follows the Langmuir adsorption isotherm model. Therefore, taking experimental data of different weigh adsorbent with fixed initial concentration result in different adsorptive equilibrium concentration into the Langmuir adsorption equation for isothermal were shown in Figure 14 Q_0 and *b* were calculated from the slope and intercept of the plots and were found to be 8.33; $2.09 \cdot 10^{-4}$, respectively.

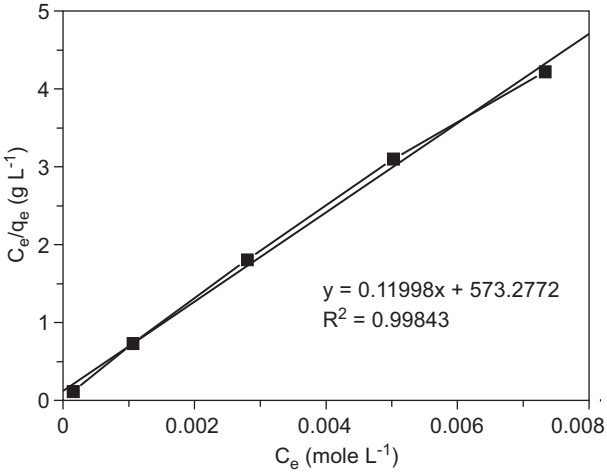

Figure 14. Langmuir adsorption isothermal or cesium ions adsorption on the MK21-KC41.

The essential characteristics of a Langmuir isotherm could be described in the terms of a dimensionless constant separation factor or equilibrium R_L which is defined by [32]

$$R_L = \frac{1}{1 + bC_0} \quad (5)$$

where C_0 is the initial cesium ion concentration (mol·l^{-1}) and *b* is the Langmuir constant related to the energy of adsorption.

Table 1. RL values and isotherms.

RL value	Type of isotherm
RL > 1	unfavourable
RL = 1	linear
0 < RL < 1	favourable
RL = 0	irreversible

The R_L values at different concentrations are list in Table 1. Taking the energy of adsorption constant b data into equilibrium R_L could be evaluated (0.99). The R_L value ($0 < R_L < 1$) indicated that the adsorption of cesium ion by MK21-KC41 is favorable.

Freunchlich adsorption isotherm

The Freundlich equation is used for heterogeneous surface energies from the presence of different functional groups on the surface, and the various adsorbent – adsorbate interactions. In contrast to the Langmuir equation, the Freundlich isotherm assumes sorption onto sorbent surfaces, which are characterized by heterogeneous sorption sites. It also assumes that the stronger adsorption sites are occupied first and the binding strength decreases with increasing binding site occupation. The results of concentration-dependent cesium ions adsorption on MK21-KC41 were analyzed by applying the Freundlich adsorption isotherm [33] in its logariyhmic form:

$$\log Q_e = \log k + \frac{1}{n} \log C_e \qquad (6)$$

where q_e is the amount of cesium ions adsorbed at equilibrium (mole·g^{-1}), C_e is the adsorptive equilibrium concentration (mole·l^{-1}). k and $1/n$ are Freunlich constants which correspond to adsorption capacity and adsorption intensity, respectively; n (g·l^{-1}) is a measure of the deviation from the linearity of adsorption.

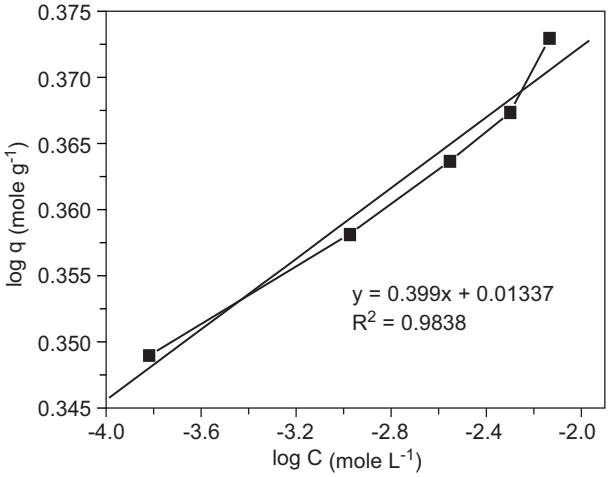

Figure 15. Freunchlich adsorption isothermal or cesium ions adsorption on the MK21-KC41.

This value indicates the degree of non-linearity between the solution concentration and adsorption as follows: if $n = 1$, the adsorption is linear adsorption process; if $n < 1$, adsorption is an unfavourable adsorption process; and if $n > 1$, adsorption is a p a favourable adsorption process.

The plot of log qe vs. log C_e was found to be linear which suggests that the adsorption of cesium ions on MK21-KC41 obeyed Freundlich adsorption isotherm over the entire range of adsorptive concentration studied. Therefore, taking experimental data of different weigh adsorbent with fixed initial concentration result in different adsorptive equilibrium concentration into the Freundlich adsorption equation for isothermal were shown in Figure 15. The $1/n$ and log k were founded from the slope and intercept of the plots to be 0.399, 0.01337, respectively. The inverse of adsorption intensity was evaluated and the result was greater than one (2.5). The result suggests that surface of the adsorbent was heterogeneous in nature with an exponential distribution of active sites [34].

CONCLUSION

Preparation of granular KZnFC via phosphoric acid-based geopolymer was carried out in this study. The granular KZnFC with the largest compressive strength value was MK51 (35.32 MPa). The improved compressive strength was due to the excess residual MgO particles. However, MK51 exhibits the lowest adsorption capacity (1.32 meq·g^{-1}) due to its lowered porous structure. To optimize both the adsorption capacity and the mechanical stability, only MK21 (1.47 meq·g^{-1}) and MK31 (1.35 meq·g^{-1}) were selected to run column operations. The performances of both granular KZnFCs were comparable to that of commercial granular inorganic adsorbent (DT-30A, 1.45 meq·g^{-1}). To improve the adsorption efficiency of MK21 and MK31, KZnFc content was increased. However, excess KZnFc content did not benefit granular KZnFC's adsorption efficiency due to the limited pore sites on the adsorbent. As a result, the optimal KZnFC-to-geopolymer ratio in achieving maximum adsorption capacity was 1.4 for MK21-KC41, and 1.2 for MK31-KC21. In addition, the adsorption of cesium ion for MK21-KC41with various contacting time was examined at different concentrations of Cs (10 ppm, 100 ppm, 1000 ppm, 2000 ppm). The adsorption efficiency remained constant after the equilibration time of 60 min. Moreover, the adsorption behavior of cesium ion on MK21-KC41 can be described by both the Langmuir adsorption equation and the Freundlich adsorption equation.

REFERENCES

1. Todd T. A., Brewer K. N., Wood D. J., Tullock P. A., Mann N. R., Olson L. G.: Separation Science and Technology *36*, 999 (2001).
2. Loos-Neskovic C.: Talanta *31*, 1133 (1984).
3. Harjula R., Lehto J., Tusa E. H., Paavola A.: Nuclear technology *107*, 272 (1994).

4. Konecny C., Caletka R.: J. Radioanal. Chem. *14*, 255 (1973).
5. Taj S., Muhammad D., Chaudhry M. A., Mazhar M.: Journal of Radioanalytical and Nuclear Chemistry 288, 79 (2010).
6. Mimura H., Kimura M., Akiba K., Onodera Y.: Separation Science and Technology 34, 17 (1999).
7. Mimura H., Kimura M., Akiba K., Onodera Y.: Journal of Nuclear Science and Technology *36*, 307 (1999).
8. Rao S. V. S., Lal K. B., Narasimhan S. V., Ahmed J.: Journal of Radioanalytical and Nuclear Chemistry *240*, 269 (1999).
9. Someda H. H., ElZahhar A. A., Shehata M. K., El-Naggar H. A.: Separation and Purification Technology *29*, 53 (2002).
10. Wagh A. S., Jeong S.-Y., Singh D. in: Proc. First Intl. Conf. on High Strength Concrete, Eds. A. Azizinamini, D. Darwin, and C. French, p. 542-553, Am. Soc. Civil Eng, 1997.
11. Singh D., Mandalika V. R., Parulekar S. J., Wagh A. S.: Journal of Nuclear Materials *348*, 272 (2006).
12. Torras J., Buj I., Rovira M., de Pablo J.: Journal of hazardous materials *186*, 1954 (2011).
13. Davidovits J. in: First international conference on alkaline cements and concretes, p. 131-149, 1994.
14. Liu L.-p., Cui X.-m., He Y., Liu S.-d., Gong S.-y.: Materials Letters *66*, 10 (2012).
15. Robuck S. J., Luthy R. G.: Water Science & Technology *21*, 547 (1989).
16. Wagh A., Singh D., Jeong S., Strain R.: *Ceramicrete stabilization of low-level mixed wastes-a complete story*, Argonne National Lab., IL (United States). Funding organisation: USDOE Office of Environmental Restoration and Waste Management, Washington, DC, United States 1997.
17. Vlasselaer S., D'Olieslager W., D'Hont M.: Journal of Inorganic and Nuclear Chemistry *38*, 327 (1976).
18. Wang A. J., Yuan Z. L., Zhang J., Liu L. T., Li J. M., Liu Z.: Mater. Sci. Eng. C Mater. Biol. Appl. *33*, 5058 (2013).
19. Mimura H., Lehto J., Harjula R.: Journal of Nuclear Science and Technology *34*, 607 (1997).
20. Loos-Neskovic C., Fedoroff M., Mecherri M. O.: The Analyst *115*, 981 (1990).
21. Li B., Liao J., Wu J., Zhang D., Zhao J., Yang Y., et al., Nuclear Science and Techniques *19*, 88 (2008).
22. Buj I., Torras J., Casellas D., Rovira M., de Pablo J.: J. Hazard. Mater. *170*, 345 (2009).
23. Ding Z.: *Research of magnesium phosphosilicate cement*, 2005.
24. Mel'gunov M. S., Fenelonov V. B., Mel'gunova E. A., Bedilo A. F., Klabunde K. J.: The Journal of Physical Chemistry B 107, 2427 (2003).
25. Lehto J., Pettersson M., Hinkula J., Räsänen M., Elomaa M.: Thermochimica Acta *265*, 25 (1995).
26. Jung H. S., Lee J.-K., Kim J.-Y., Hong K. S.: Journal of Colloid and Interface Science *259*, 127 (2003).
27. Holgado M.: Solid State Ionics *92*, 273, (1996).
28. Banks E., Chianelli R., Korenstein R.: Inorganic Chemistry *14*, 1634 (1975).
29. Lawn B. R.: *Fracture of brittle solids,* Cambridge university press, 1993.
30. Lin Y., Fryxell G. E., Wu H., Engelhard M.: Environmental Science & Technology *35*, 3962 (2001).
31. Langmuir I.: Journal of the American Chemical Society *40*, 1361 (1918).
32. Hall K. R., Eagleton L. C., Acrivos A., Vermeulen T.: Industrial & Engineering Chemistry Fundamentals *5*, 212 (1966).
33. Freundlich H. M. F.: The Journal of Physical Chemistry *57*, 385 (1906).
34. Sips R.: The Journal of Chemical Physics *16*, 490 (1948).